Journal of the Taiwan Institute of Chemical Engineers 131 (2022) 104141

Contents lists available at ScienceDirect

Journal of the Taiwan Institute of Chemical Engineers

journal homepage: www.elsevier.com/locate/jtice

Effect of hydrodynamic heterogeneity on particle dispersion in a Taylor-Couette flow reactor with variable configurations of inner cylinder

Lu Liu[a,b], Xiaogang Yang[c,*], Jie Yang[d], Guang Li[c], Yanqing Guo[c], Guichao Wang[a,b], Lian-Ping Wang[a,b]

[a] Guangdong Provincial Key Laboratory of Turbulence Research and, Applications, Center for Complex Flows and Soft Matter Research and, Department of Mechanics and Aerospace Engineering, Southern University of Science and Technology, Shenzhen 518055, P.R. China
[b] Guangdong-Hong Kong-Macao Joint Laboratory for Data-Driven Fluid Mechanics, and Engineering Applications, Southern University of Science and Technology, Shenzhen 518055, Guangdong, China
[c] Department of Mechanical, Materials and Manufacturing Engineering, University of Nottingham Ningbo China, Ningbo 315100, P.R. China
[d] Department of Physics & Mathematics, University of Hull, Hull HU6 7RX, UK

ARTICLE INFO

Article History:
Received 22 June 2021
Revised 18 October 2021
Accepted 6 November 2021
Available online 23 November 2021

Keywords:
multiphase flow model
Taylor-Couette flow reactor, Eulerian-Lagrangian approach
particle dispersion

ABSTRACT

Background: Effect of hydrodynamic heterogeneity on particle dispersion in a Taylor-Couette flow (TC) reactor with variable configurations of inner cylinder has been investigated using CFD modelling.
Methods: Particle dispersion was tracked based on the Eulerian-Lagrangian approach, where the reactant solution phase was solved in the Eulerian reference frame, while the particle dispersion was calculated by tracking a large number of particles with consideration of the hydrodynamic forces acting on particles and adopting actual particle properties measured from the particle synthesis experiments.
Significant Findings: The simulation reveals that particle dispersion is significantly enhanced by increasing the inner cylinder rotational speed, characterized by particle distribution for both circular inner cylinder Taylor-Couette flow reactor (CTC) and lobed cross-section inner cylinder Taylor-Couette flow reactor (LTC). Particle trajectories or dispersion are influenced by the turbulent Taylor vortices. Particle radial dispersion affects the particle classification by presenting different particle axial velocities in radial direction, while particle axial dispersion can be seen as an indicator for global mixing occurring in the TC reactor, which is enhanced at high rotational speed, especially in the LTC. The calculated dispersion coefficient is found to be similar to the shape of particle size distribution found in the experiments.
© 2021 The Author(s). Published by Elsevier B.V. on behalf of Taiwan Institute of Chemical Engineers. This is an open access article under the CC BY-NC-ND license (http://creativecommons.org/licenses/by-nc-nd/4.0/)

1. Introduction

The synthesis of fine particles depends on the dispersion of primary particles. This can be achieved through the interaction between fluid flow and particles, where turbulent shear acts to aggregate primary particles forming larger clusters or causes breakage of already formed agglomerates. During this procedure, particle properties are changed, being strongly dependent on the applied shear rate. In the literature, various studies exist addressing the effect of the shear intensity on particle size and shapes using different reactors [1–3]. In these studies, the resulting particle populations are analysed by considering the volume average shear rate, $\langle G \rangle = \sqrt{\langle \varepsilon \rangle / \nu}$, obtained from the power input, which usually serves as the characteristic quantity of the flow field. However, in reality for a given reactor, shear rate often exhibits a distinct distribution, which has a significant impact on the particle dispersion [4,5]. As both aggregation and breakage of particles in the dispersion are strongly dependent on the shear rate, the effect of the heterogeneity of the local shear rate on particle dispersion needs to be considered.

The generation of Taylor vortices is the most distinct feature in the Taylor-Couette flow (TC) reactor. Such vortices often occur in pairs in the gap area and vary due to the sensitivity to many influence factors, such as the reactant fluid property, inner cylinder geometry and rotational speed. Previous studies, for example, Snyder [6]; Lathrop *et al.* [7] and Ehrl *et al.* [8] among others have summarized a series of instabilities driven by the centrifugal force when the Reynolds number or Taylor number exceeds a critical value to yield Taylor vortices. The heterogeneity in the TC reactor will experience the flow pattern change from Taylor vortex flow, wavy Taylor vortex flow, modulated wavy Taylor vortex flow, turbulent Taylor vortex flow to fully developed Taylor flow. Experimentally, Vaezi *et al.* [9] have measured the intensity of turbulent velocity fluctuation in a TC reactor by means of Laser-Doppler velocimetry (LDV) and Wang *et al.* [10] and Tokgoz *et*

* Corresponding author: Tel: +86-574-88182419
E-mail address: Xiaogang.Yang@nottingham.edu.cn (X. Yang).

https://doi.org/10.1016/j.jtice.2021.11.008
1876-1070/© 2021 The Author(s). Published by Elsevier B.V. on behalf of Taiwan Institute of Chemical Engineers. This is an open access article under the CC BY-NC-ND license (http://creativecommons.org/licenses/by-nc-nd/4.0/)

Nomenclature

C_D	drag coefficient
d_p	particle size, m
$\overline{d}_p$	size constant
D	gap width, m
d_{ij}	deformation tensor
Dz	diffusion coefficient, m^2/s
$\mathbf{F}_{P\text{-}L}$	external force, $kg/(m^2 \cdot s^2)$
g	gravity, m/s^2
k	turbulent kinetic energy, m^2/s^2
L	reactor length, m
$\dot{m}_p$	mass flow rate of particles, kg/s
n	size spread parameter
N	total number of particles
p	pressure, Pa
r_i	radius of the inner cylinder, m
r_o	radius of the lobed outer cylinder, m
Re	Reynolds number
Re_p	particle Reynolds number
St_η	Stokes number
$\mathbf{u}_L$	instantaneous velocity, m/s
u'_L	velocity fluctuation, m/s
u_{L}	Reynolds-average velocity, m/s
$\mathbf{u}_P$	particle velocity, m/s
Y_d	accumulated mass fraction of particle
z_i	axial position of the i^{th} particle

Greek letters

ε	turbulent energy dissipation rate, m^2/s^3
ν	kinematic viscosity of the fluid, m^2/s
ρ_L	liquid density, kg/m^3
ρ_p	particle density, kg/m^3
τ_L	stress tensor, $kg/(m \cdot s^2)$
τ_p	particle relaxation time, s
τ_f	characteristic time of flow, s
ω_i	angular velocity, rad/s
Ω	rotational speed of the inner cylinder, rpm
μ	molecular viscosity, kg/(m·s)

al. [11] have adopted the particle image velocimetry (PIV) to measure the velocity field data. Numerically, CFD modelling has been widely adopted to obtain the important information of the fluid flow in the TC reactor, especially for the turbulence which has a dominant effect on the particle dispersion. Such numerical simulations can be found, for example, by using the Reynolds stress model [12,13], and by employing the large eddy simulation (LES) [14]. For numerical modelling of the particle dispersion in the TC reactor, Chouippe *et al.* [15] have investigated the dispersion behaviour of bubbles in turbulent Taylor-Couette flow, revealing the phenomenon of the preferential accumulation of bubbles. Wang *et al.* [16] used *k*-ε model coupled with PIV validation and the quadrature method of moments (QMOM), to predict the mean particle size of latex spheres under the effect of local fluid shear in turbulent Taylor-Couette flow. Dutta and Ray [17] utilized the Taylor-Couette flow to realise water purification. As the Taylor-Couette flow has a feature of narrow shear rate distribution, the application of such flow can facilitate particle classification to acquire uniform particle size so that the particle rheological behaviour and other properties can be changed accordingly. Also, when the density difference between the particles and the fluid is small, shear-induced particle migration under the influence of Taylor vortices will be beneficial to the classification of particle size [18]. This is strongly associated with the dispersion of particles in the TC reactor. Ohmura *et al.* [19] have successfully realized the classification of particles with various sizes using the TC reactor, validated by both numerical simulation and the actual experiments. They have observed that large particles, which are located near the edges of Taylor vortex, tend to be transported downward or upward due to the effect of outward and inward impinging jet flows formed in the regions between the Taylor vortices, while small particles are mainly remained in the core of vortices.

Taylor-Couette turbulent flow has been recognised as an effective way for the synthesis of various particles due to its shear controllable feature. Jung *et al.* [20] prepared calcium carbonate ($CaCO_3$) particles using a TC reactor. The synthesised $CaCO_3$ agglomerates present various sizes and morphologies when changing the operating conditions such as reactant flow rate, concentration and angular velocity of inner cylinder. They also compared the particles synthesized using the TC reactor with those using a stirred tank. Interestingly, they reported that the adoption of TC reactor may be appropriate to obtain particles of smaller size with a uniform shape due to rather homogenous mixing conditions available in such reactor. Nguyen *et al.* [21,22] employed a TC crystallizer, working in a continuous mode with multiple feeding mode to obtain guanosine 5-monophosphate (GMP) crystals. They observed that the phase transformation of GMP in the TC crystallizer is about ten times faster than that in the conventional stirred tank crystallizer. They have attributed this phenomenon to the optimal control of the mass transfer rate and mean residence time in the TC crystallizer. In the fabrication of lithium-ion batteries, the TC crystallizer can be seen as an effective device to synthesize precursors of cathode materials for lithium-ion batteries, such as $Ni_{1/3}Co_{1/3}Mn_{1/3}(OH)_2$ [23], and $Ni_{0.9}Co_{0.05}Mn_{0.05}(OH)_2$ according to a series of studies by Kim *et al.* [3,24], and the most promising core-shell structure [25]. The synthesized secondary particles were found to exhibit good properties in terms of tap density, particle size, and morphology. It is deduced that under the effect of Taylor vortices, the exposure of agglomerates to local turbulence induced shear will be beneficial to spherical particle growth and formation of the dense structure. It should be noted that these studies are mainly focused on the experimental preparation of particles, while the interaction of turbulence and particles is not fully investigated. In order to explain the results of particle properties, they generally used the empirical correlations between the particle size and flow shear generated by Taylor vortices. So far, limited work has been conducted in relation to how the hydrodynamics, especially the turbulent flow field, in a TC reactor influences the particle formation and dispersion. Nemri *et al.* [26] used Kalliroscope AQ-1000 flakes to observe flow pattern in the TC reactor, and the flake trajectory was used to observe the inter-vortex mixing, but their simulation was carried out with single phase flow, and these particles were neutral particles without true attributes. We cautiously point out that it is the local hydrodynamics that provides the environment for particle nuclei to interact with the turbulent eddies, consequently bringing out the particle formation and growth. These mentioned studies lack the interpretation of the interaction mechanism between the local turbulent flow and the formed particle dispersion.

In the present study, we investigate the barium sulfate particle dispersion in the TC reactor with variable configurations of inner cylinder, taking into account the momentum exchange between carrier fluid and particles. The properties of these particles are set similar to those obtained from our previous experimental results, including particle density, particle size, and its distribution [27]. The parameters that influence the particle dispersion will be assessed, including the rotational speed (or characterized by the Reynolds number) and the configuration of the inner cylinder, where circular and lobed cross-sectional profiles are concerned. The flow field information is firstly obtained by CFD modelling, and then the tracking of particle trajectory will be realized by using Eulerian-Lagrangian method (discrete phase model) with two-way coupling. This paper will be organised as follows. Section 2 will present the theoretical background and

modelling details for evaluating fine particle dispersion in the TC reactor system, while Section 3 will present the results and discussion on the particle dispersion behaviour and the likely implication for the synthesis of fine particles using the TC reactor. Finally, Section 4 will summarise the conclusions derived from the study.

2. Mathematical modelling

The hydrodynamics in the TC reactor can be described by the existing two-phase flow model, which consists of a continuous liquid phase (i.e., the reactant solution), and a certain amount of suspended particles, usually measured by the volume fraction. As the volume fraction of the dispersed particles in the experiments is smaller than 10%, the adoption of Eulerian-Lagrangian approach is deemed appropriate for the description of particle dispersion. Also, the use of Lagrangian framework allows for the rigorous tracking of the movement of individual particles so that the dispersion can be well defined based on the statistics of the particle trajectories, and forces acting on particles can be identified separately by considering particle motion characteristics [28]. In the meantime, the particle size distribution, which is important in determining particle characteristics, can be implemented into the numerical simulation, yielding a better prediction for particle dispersion [29,30].

2.1. Governing equations

2.1.1. Liquid phase

As the effect of hydrodynamic heterogeneity on particle dispersion in the TC reactor is studied, the appropriate description of the interaction between continuous phase and discrete phase is crucial and two-way coupling has to be considered. Thus, the conservation equations for continuous phase are given by

Continuity equation:

$$\nabla \cdot (\alpha_L \rho_L u_L) = 0 \tag{1}$$

Momentum conservation equation:

$$\frac{\partial}{\partial t}(\alpha_L \rho_L u_L) + \nabla \cdot (\alpha_L \rho_L u_L u_L) = -\nabla p + \nabla \cdot (\alpha_L \tau_L) + \alpha_L \rho_L g + F_{P-L} \tag{2}$$

where α_L is the liquid phase volume fraction and $\alpha_L = 1 - \alpha_P$, u_L is the Reynolds-average velocity, $\rho_L$is the liquid density, p is the static pressure, τ_L is the stress tensor, $\rho_L g$ is the gravitational force, and F_{P-L} is the forces acting on the liquid phase due to the particles, which arises from the interaction with the dispersed particles.

In order to determine the flow pattern in the TC reactor, a Reynolds number has been defined, expressed as

$$Re = \frac{\omega_i r_i d}{\nu} \tag{3}$$

where ω_i and r_i are the angular velocity and the radius of the inner cylinder, respectively. For the LTC, r_i will be replaced by the equivalent or hydraulic radius of the inner cylinder. d is the gap size, and ν is the kinematic viscosity of fluid. The minimum rotational speed is 300 rpm, corresponding to the Reynolds number of 12324. Based on the classification of flow pattern in the TC reactor [7], all operating conditions are under turbulent flow. Thus, it would be safe to employ the RNG k-ε turbulence model in the simulation as the flow in the TC reactor has the feature of swirling [31]. However, the entrained particles by Taylor vortices will have the impact on the reactant liquid turbulent kinetic energy and distribution of turbulent energy dissipation rate. Such effect has been considered by adding the source terms into the RNG k-ε model. When the volume fraction of the dispersed particles is very small, turbulence modulation by dispersed phase is weak. In such case, the RNG k-ε equations can be simplified and their original forms without including source terms are adopted.

k equation:

$$\frac{\partial}{\partial t}(\rho k) + \nabla \cdot (\rho k u_L) = \nabla \cdot \left(\frac{\mu_{eff}}{\sigma_k} \nabla k\right) + G_k - \rho\varepsilon \tag{4}$$

ε equation:

$$\frac{\partial}{\partial t}(\rho \varepsilon) + \nabla \cdot (\rho \varepsilon u_L) = \nabla \cdot \left(\frac{\mu_{eff}}{\sigma_\varepsilon} \nabla \varepsilon\right) + C_{1\varepsilon}\frac{\varepsilon}{k} G_k - C_{2\varepsilon}\rho\frac{\varepsilon^2}{k} - R_\varepsilon \tag{5}$$

where k is the turbulent kinetic energy, ε is the turbulent energy dissipation rate, μ_{eff} is the effective viscosity, σ_k and σ_ε are turbulent Prandtl numbers, G_k is the generation of turbulent kinetic energy, $C_{1\varepsilon}$ and $C_{2\varepsilon}$ are model constants, and R_ε is the extra strain rate [32]. The definition of these terms or functions can be referred to Liu *et al.* [27]. Additionally, as all operating conditions are in turbulent flow, in order to distinguish turbulent degree related to particle synthesis in the present work, turbulent energy dissipation rate is provided in Figure S1 of the supplementary material based on our preliminary work.

2.1.2. Dispersed phase

The dispersed particle tracking is conducted in a Lagrangian reference frame, where individual particle trajectories can be tracked by solving the particle equation of motion. The particles are divided into several particle size bins according to the experimentally obtained particle size distribution. The positions of particles can be obtained from the following equation:

$$\frac{dx_p}{dt} = u_p \tag{6}$$

The velocity of particles u_p can be obtained by solving the force balance equation:

$$\frac{du_p}{dt} = F_D(u_L - u_p) + F_L(u_L - u_p) + \frac{g\left(\rho_p - \rho_L\right)}{\rho_p} \tag{7}$$

where ρ_p is the density of particles. As the density of barium sulfate particles (4500 kg/m^3) is much larger than that of the reactant liquid (about 998.2 kg/m^3), the drag force will be dominant and the added mass force can be ignored. The lift force is still considered as particles are subjected to strong shear induced by the Taylor vortices and embedded turbulent eddies in the TC reactor. The drag force factor F_D can be estimated using Equation (8):

$$F_D = \frac{18\mu}{\rho_p d_p^2}\frac{C_D Re_p}{24} \tag{8}$$

where μ is the liquid viscosity, C_D is the drag coefficient, d_p is the particle diameter, and Re_p is the Reynolds number based on the particle diameter, given by

$$Re_p = \frac{\rho d_p \left|u_p - u_L\right|}{\mu} \tag{9}$$

It is assumed that barium sulfate particles can be treated as smooth spherical particles. Then, the drag coefficient, C_D can be estimated using the following expression,

$$C_D = a_1 + \frac{a_2}{Re_p} + \frac{a_3}{Re_p^2} \tag{10}$$

where a_1, a_2, and a_3 are constants, depending on the value of Re_p. Details can refer Morsi and Alexander [33]. With respect to the lift force factor, the Saffman's lift force model is adopted, given by

$$F_L = \frac{2K\nu^{1/2}\rho d_{ij}}{\rho_p d_p (d_{lk} d_{kl})^{1/4}} \tag{11}$$

where K is a constant, equal to 2.594, and d_{ij} is the deformation tensor. Equation (7) is the ordinary differential equation for description

of movement of individual particles and can be solved by integration over discrete time steps, yielding the predicted particle trajectories. It should be noted that the time step taken in the integration should be smaller than the typical turbulence integral time scale for turbulent eddies in the TC reactor. Therefore, during the calculation, the rule of thumb used for modelling the continuous phase is that the time step used for transient simulation is at least 10 times greater than that for the dispersed particle tracking. In order to capture the effect of turbulence on the particle dispersion, stochastic tracking model is employed. Because this model takes the instantaneous turbulent velocity fluctuation, u_L' at the location of the particle, the instantaneous velocity for the continuous phase at particle position is given by

$$u_L = u_L + u_L' \tag{12}$$

Since the turbulent kinetic energy at particle position in the flow can be obtained, the root mean square value of each fluctuating component u_L' can be approximated by

$$\sqrt{\overline{u_{L\theta}'^2}} = \beta_1\sqrt{k},\ \sqrt{\overline{u_{Lr}'^2}} \approx \sqrt{\overline{u_{Lz}'^2}} = \beta_2\sqrt{k} \tag{13}$$

where β_1 and β_2 are the constants that can be used to account for the non-isotropic distribution of the shear turbulence in the TC [9,34,35]. It is found that the values of β_1 and β_2 are about 1.2 and 0.8, respectively.

2.1.3. Momentum source term

Momentum is exchanged during the interaction of continuous phase and discrete phase. The momentum source term arises from the forces exerting on individual particles. As it has been indicated above, drag force, and lift force are dominant forces for the currently investigation system, therefore, the momentum exchange can be expressed by the following equation,

$$F_{P-L} = \sum\left[\frac{18\mu}{\rho_p d_p^2}\frac{C_D Re_p}{24}(u_L - u_p) + \frac{2K\nu^{1/2}\rho d_{ij}}{\rho_p d_p (d_{lk}d_{kl})^{1/4}}(u_L - u_p)\right]\dot{m}_p\Delta t \tag{14}$$

where $\dot{m}_p$ is the mass loading of particles. The mass loading has been assumed to be uniform and equal to the inlet mass flow rate.

2.2. Particle size distribution

In our previous study [27], particles were continuously taken from the reactor after one time of the average residence time t_{res}, where $t_{res} = \frac{V}{Q}$ (V: the volume of the reactor; Q: the volumetric feeding rate). Particle size distribution was then measured by using Malvern Mastersizer, and the average size (D50) was adopted to characterize the average particle size. These experimental data of particle size distributions at different Reynolds numbers are directly used in the particle inlet. During the calculation, the particle size distribution is assumed to follow the Rosin-Rammler distribution, where the mass fraction of those particles, whose diameter is greater than d_p is given by

$$Y_d = e^{-\left(d_p/\overline{d}_p\right)^n} \tag{15}$$

where Y_d is the accumulated mass fraction for particles with the diameter greater than d_p, $\overline{d}_p$ is the size constant, and n is the size spread parameter. Once the particle size is classified into several discrete diameter groups, the mass fraction of each group can be obtained accordingly. In order to determine the values of parameter n, and $\overline{d}_p$, Equation (15) can be converted to a linear format by taking the logarithm operation for both sides of the equation, yielding

$$\ln(-lnY_d) = nlnd_p - nln\overline{d}_p \tag{16}$$

Based on the fitted straight line, the value of n can be obtained from the slope while the value of $\overline{d}_p$ can be obtained from the intercept.

2.3. Initial and Boundary conditions

For the continuous phase, the inlet and outlet boundary conditions were set as the velocity inlet and pressure outlet, respectively. Hydraulic diameter of the inlet was specified while the turbulent intensity was set at 5%, assuming the feeding to be smooth. No-slip boundary conditions were imposed to all the inner cylinder and outer cylinder surfaces and the standard wall functions were applied to the meshes close to the inner and outer cylinder surfaces. As the present work mainly focuses on the investigation of the effect of rotational speed, the minimum solution feeding rate (i.e., 10 mL/min) used in our previous experiment [27] was chosen, corresponding to an axial velocity component of 1.22×10^{-4} m/s caused by feeding. Figure S2 in the supplementary material shows the preliminary result of axial velocity, whose magnitude is much larger than the feeding velocity. Therefore, such small solution feeding rate almost have little disturbance to the flow.

For the discrete phase, particle parcels were injected from the inlet surface, where the total flow rate for all particles was set based on the actual experimental results [27]. The number of particles in one parcel can be estimated by $NP = \dot{m}_s\frac{\Delta t_p}{m_p}$. The collision between the particles and the surfaces of the cylinder is assumed to be elastic, which can be specified as the reflect type of boundary condition. The escape boundary condition was assigned for the particle inlet and outlet to eliminate those unphysical particle trajectories. This means particles encountering the boundaries will not be accounted in the simulation and their trajectory calculations will be terminated.

2.4. Physical TC reactor model

The configuration of the TC reactor is depicted in Figure 1 (a), and its dimensions are listed in Table 1. Based on the previous study of the preparation of barium sulfate particles [27], it has been demonstrated that a modified geometry of inner cylinder from the traditional circular one (CTC) to a lobed one (LTC) can effectively intensify the local turbulence, beneficial to the particle aggregation. The supporting evidence can be seen from Figure S3 in the supplementary material, where particle size and the characterization of local turbulence by energy dissipation rate are provided with similar variation trend for both reactors. Therefore, the present simulations focus on the particle behaviour in the LTC at different rotational speeds. For comparison purpose, the simulation on particle dispersion at a high rotational speed of 1000 rpm in the CTC is also conducted. Additionally, in order to ensure the consistency of particle behaviour in the CTC, Figure S4 in the supplementary material provides the results operated at 300 rpm for reference. The computational domain is shown in Figure 2. Procedures of the preparation of barium sulfate particles can be found in the study of Liu *et al.* [27].

2.5. Numerical simulation

The commercial CFD software, Fluent 18.0, was employed to simulate the particle dispersion in the TC reactor. The flow and hydrodynamic heterogeneity were described by solving the Reynolds-Average Navier-Stokes equations coupled with RNG k-ε model. Meanwhile, the particles were tracked using equation of motion as defined by Equation (7). Computational mesh was created by ANSYS ICEM with a total cell number more than 1,100,000. According to the dimensions of the TC reactor as listed in Table 1, a mesh setup with $147 \times 480 \times 16$ (circumferential $\times$ axial $\times$ radial) was adopted in the

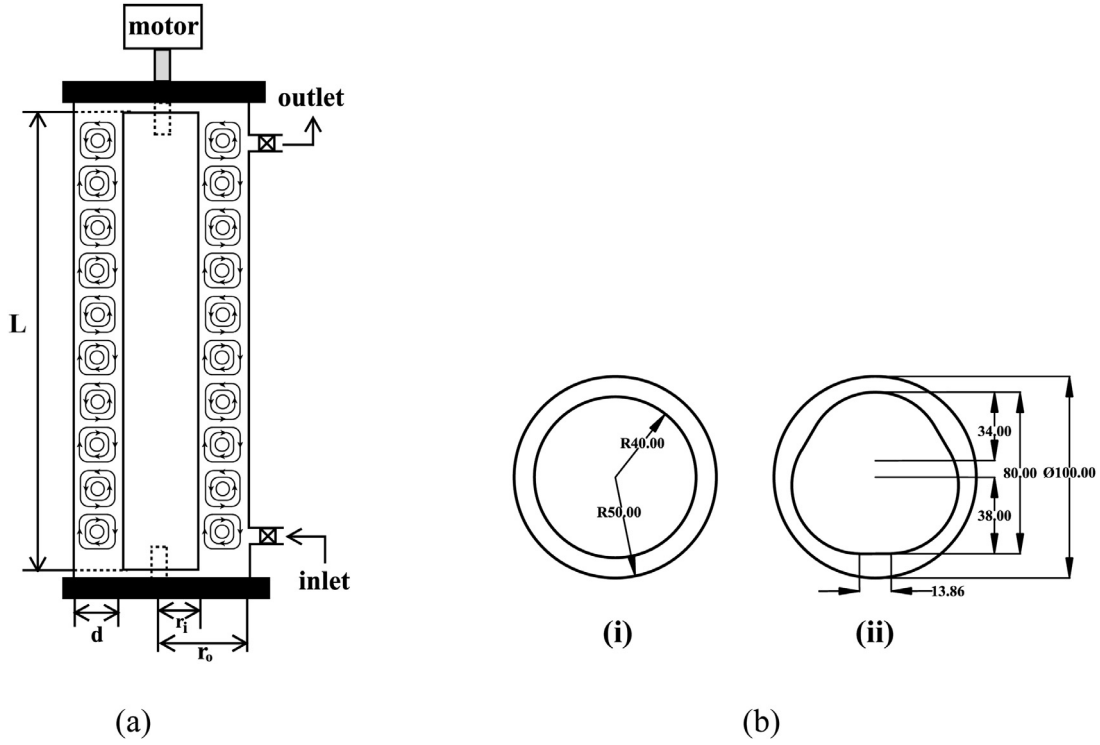

Figure 1. (a) Configuration of the TC reactor; and (b) Inner cylinder geometry for the: (i) CTC; and (ii) LTC.

numerical simulation, as illustrated in Figure 2 (a). For the inner fluid zone containing lobed inner cylinder, the mesh was additionally refined, shown in Figure 2 (b). Mesh independence check in terms of wall shear stress has been carried out to ensure the accuracy of CFD results, shown in Figure S5 in the supplementary material. Further refinement to the mesh of 147 × 480 × 25 has negligible impact on the simulation results, which indicates that the mesh size of 147 × 480 × 16 is fine enough to ensure numerical accuracy. The simulation details can be found in Liu *et al.* [27]. The pressure-velocity coupling was realized by SIMPLEC algorithm while PRESTO! Scheme was used for the pressure calculation. The second-order upwind scheme was adopted for the calculation of momentum, and the same for the calculation of turbulent kinetic energy and turbulent energy dissipation. From the trial simulation, the time step size for continuous liquid phase was set at 10^{-3} s as the Taylor vortices can be still well captured from the simulation. The particles were tracked using a time step of 10^{-5} s to ensure the particle time step size is smaller than the integration time step. The convergence criteria for all parameters were set 10^{-5} in relative scaling. Additionally, in order to ensure the CFD simulation to be able to capture major hydrodynamic features, turbulence model validation has been conducted in advance by the comparison with Haut *et al.*'s [36] experimental data, shown in Figure S6. Details are provided in the supplementary material.

Table 1
Dimensions and operating conditions of the TC reactor.

Dimension	CTC	LTC
Reactor length, L (mm)	300.00	300.00
Inner cylinder radius, r_i (mm)	40.00	40.19
Outer cylinder radius, r_o (mm)	50.00	50.00
Gap size, d (mm)	10.00	9.81
Rotational speed, Ω (rpm)	1000	300, 600, 800, 1000
Reynolds number	41680	12324, 24649, 32866, 41082

3. Results and discussion

3.1. Characterisation of particle entrainment by Taylor vortices

Under the condition of a certain Reynolds number, Taylor vortices are generated in the TC reactor, where the two adjacent vortices are counter-rotating, embedded various scales of turbulent eddies from large to Kolmogorov dissipation scale. Also, the inward and outward impinging jet flows between the two vortices are created [37]. Figure 3 shows the distribution of particles in the gap of the LTC at different rotational speeds of the inner cylinder. Colour bar denotes particle velocity magnitude. Firstly, it can be seen clearly from the figure that with increase of the rotational speed, particles are entrained and dispersed with enhanced particle velocity. Because the axial transport of the Taylor vortices (can be confirmed by the axial

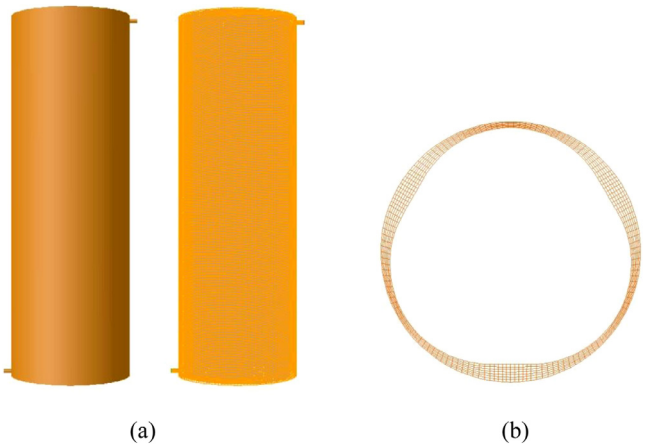

Figure 2. Mesh setup for computational domain: (a) global mesh view; and (b) mesh refinement for inner fluid zone.

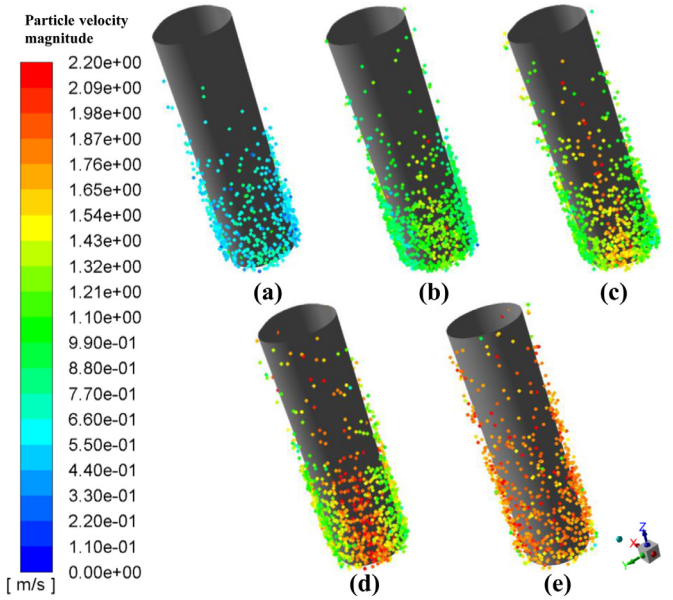

Figure 3. Particle distribution in the LTC: (a) 300 rpm; (b) 600 rpm; (c) 800 rpm; (d) 1000 rpm, and the CTC: (e) 1000 rpm.

velocity in Figure S2 of the supplementary material) will bring out the enhanced dispersion of particles across the vortices while interacting with the embedded turbulent eddies. Although the density of barium sulfate is greater than the reactant liquid, the particle size is extremely small with the order of 10^{-7} m. This results in particles to be easily suspended throughout the entire reactor as can be observed from Figure 3, especially when the LTC is working at a high rotational speed. For the given residence time, the simulation results show that the particles have not yet dispersed to across the reactor length at a rotational speed of 300 rpm while a large number of particles have been entrained to the top of the reactor at the rotational speed exceeding 800 rpm. This clearly indicates that the turbulence shear enhanced by increasing the inner cylinder of the LTC has a significant impact on particle dispersion. Secondly, it can be also observed from Figures 3 (c) and (d) that the particles with high velocity tend to distribute in the large gap regions in the LTC when working at high rotational speed. This is very likely to attribute to the fact that the impinging jet flows formed between the two deformed Taylor vortices strongly entrain the particles towards these regions. Also, the flow in circumferential direction experiences an expansion following by a contraction due to the gradually decrease gap for the LTC. Figure 3 (e) displays the particle distribution in the CTC for comparison, which shows the dispersion of particles in the CTC is more even than that in the LTC for operating the same rotational speed. Obviously, due to the axisymmetric feature of the CTC and the uniformly distributed radial circumferential velocity gradient, the external forces exerted on the particles ensure that particles are dispersed relatively uniform in the circumferential direction. In contrast, the radial circumferential velocity gradient in the LTC will experience the periodic change due to the deformed Taylor-vortices, thus causing the particles to disperse towards the large gap regions.

3.2. Particle trajectory

In order to observe the interaction of particles with Taylor vortex, particles are tracked at a specified time interval. Figure 4 illustrates the predicted particle trajectory for the inner cylinder operating at 1000 rpm in the CTC and LTC, respectively. Here two representative trajectory paths are randomly selected for each reactor, and the colour bar denotes fluid velocity magnitude. It should be mentioned here that the trajectories shown in the CTC and LTC could be not selected with the same particle size, and the hydrodynamic conditions are different in both reactors. Firstly, it can be seen from the streamlines created along the vertical cutting plane that the velocity magnitude is enhanced in the large gap region for the LTC in comparison to the CTC, consistent with the argument of Soos *et al.* [38] that the heterogeneity in the TC reactor can be improved by varying the configuration of the inner cylinder. The main advantage of the LTC is that Taylor-Couette flow feature is still remained but the low velocity regions are reduced. Secondly, it can be seen from the fluid streamline in the vertical cutting plane that particles injected from the inlet are entrained by Taylor vortices, and will have strongly interaction with the embedded eddies. As a result, particles are subsequently dispersed to follow a helical movement behaviour. The local amplified images with the arrow line clearly indicate the direction of particle entrainment.

It can be seen from Figure 5 that the high total pressure appears in the regions between two adjacent vortices, especially in large gap region in the LTC. This is in agreement with the particle distribution shown in Figure 3, where particles with high velocity are likely to appear in the large gap region. However, it is contradicted with the expectation that the particles do not significantly accumulate in those low pressure regions, especially the small gap region in the LTC. This is likely caused by the change of dominating force in the gap of the TC reactor. In Qiao *et al.*'s [39] study, they observed that light particles are easy to be trapped on the wall of the inner cylinder. Along the radial direction, the pressure force exerted on the particles is 6 times greater than the centrifugal force at low Reynolds numbers, which favourably drives the particles migrating towards the inner cylinder surface. With the increase in Reynolds number, the drag force exerted on the particles increases, which enhances the capability of the vortices to entrap the particles. While for heavy particles, their study found that they are trapped in the regions around the inner cylinder. This phenomenon can be interpreted by discussing the trapping of particles by Taylor vortices, which is characterized by Stokes number:

$$St_\eta = \frac{\tau_p}{\tau_f} \tag{17}$$

where τ_p is the particle relaxation time, and τ_f is the characteristic time of the local flow of Kolmogorov scale turbulent eddies. τ_p and τ_f can be estimated by the following equations

$$\tau_p = \frac{\rho_p d_p^2}{18\mu} \tag{18}$$

$$\tau_f = \sqrt{\frac{\nu}{\varepsilon}} \tag{19}$$

As suggested by Crowe *et al.* [40], if $St < 1.0$, particles will closely follow the fluid flow. In the present study, this indicates that the particles are entrapped by turbulent eddies, which are embedded in the Taylor vortices, and then strongly interact with those eddies. On the contrary, if $St_\eta > 1.0$, particles are dominated by their inertia, and they cannot respond immediately to the change of turbulent eddies. Figure 6 shows the Stokes number at different rotational speeds by using the average particle size obtained from the experimental results under the respective condition [27]. It can be seen clearly that at all the range of rotational speeds, the Stokes number, St_η, has the order of 10^{-4}, indicating the entrapment of particles by the turbulent eddies, being consistent with the observation of the particle trajectories as shown in Figure 4.

3.3. Particle dispersion in radial direction

As can be seen from the aforementioned results, particle trajectories are influenced by Taylor vortices in the TC reactor. In order to observe the particle dispersion in radial direction, a horizontal

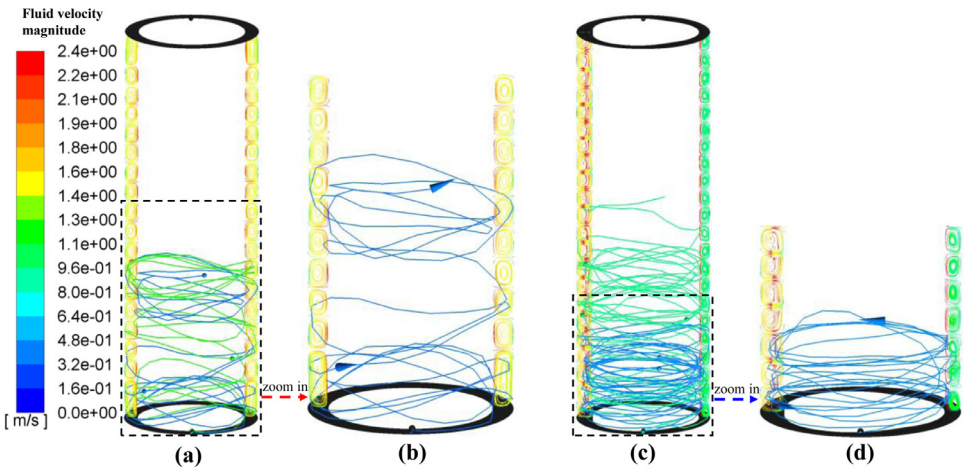

Figure 4. Particle trajectory at 1000 rpm in the: (a) CTC; (b) local enlargement of the CTC; (c) LTC; and (d) local enlargement of the LTC.

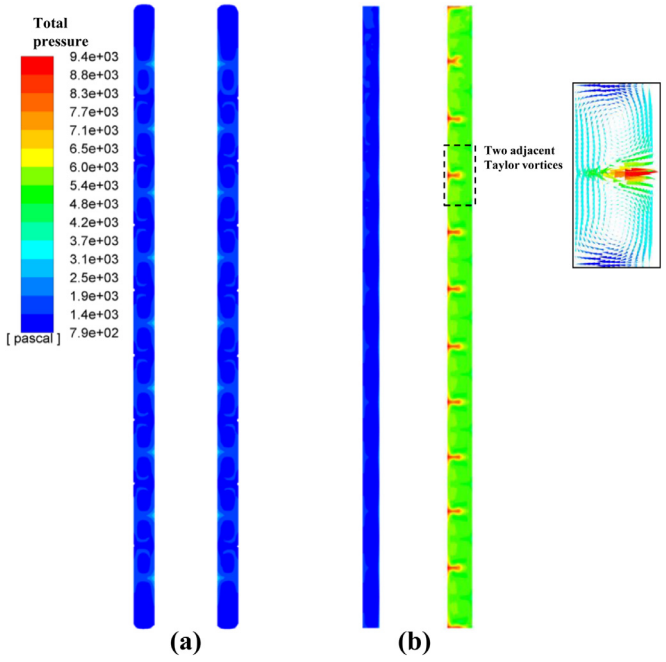

Figure 5. Total pressure distribution at 1000 rpm in the: (a) CTC; and (b) LTC.

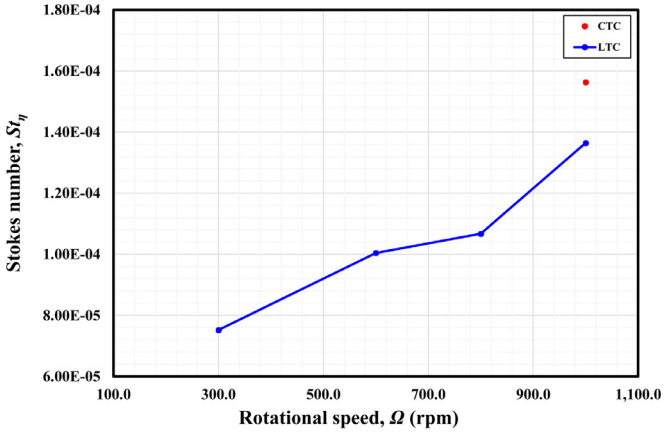

Figure 6. Stokes number at different Reynolds numbers.

cutting plane was created, as displayed in Figure 7. Colour bar denotes the axial velocity magnitude of the particles. It can be seen from the figure that with increase of the rotational speed, the downward and upward axial velocity of the vortices increase. Secondly, the particles with low slip velocity tend to distribute near the core of vortices while those with high slip velocity distribute near the wall of either inner cylinder or outer cylinder. It seems that there exists a separation strap of the particles inside and outside the vortices. The

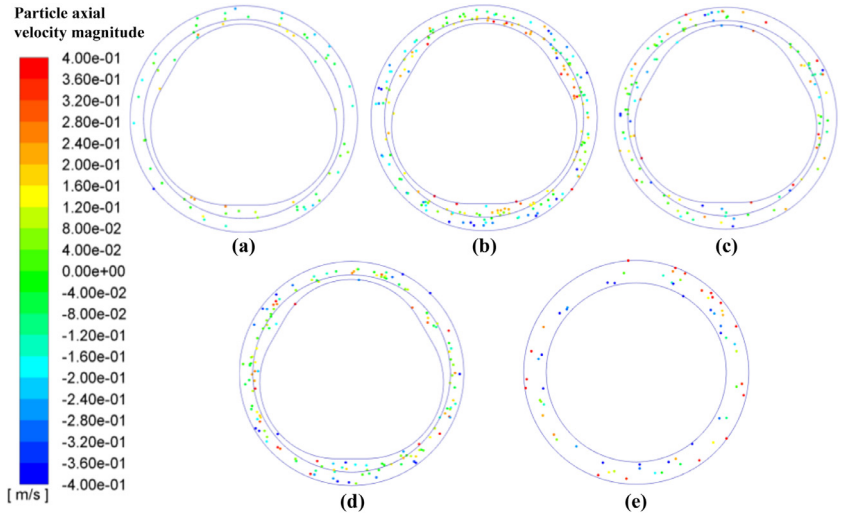

Figure 7. Particle distribution in terms of axial velocity in horizontal cutting plane of the LTC: (a) 300 rpm; (b) 600 rpm; (c) 800 rpm; (d) 1000 rpm, and the CTC: (e) 1000 rpm.

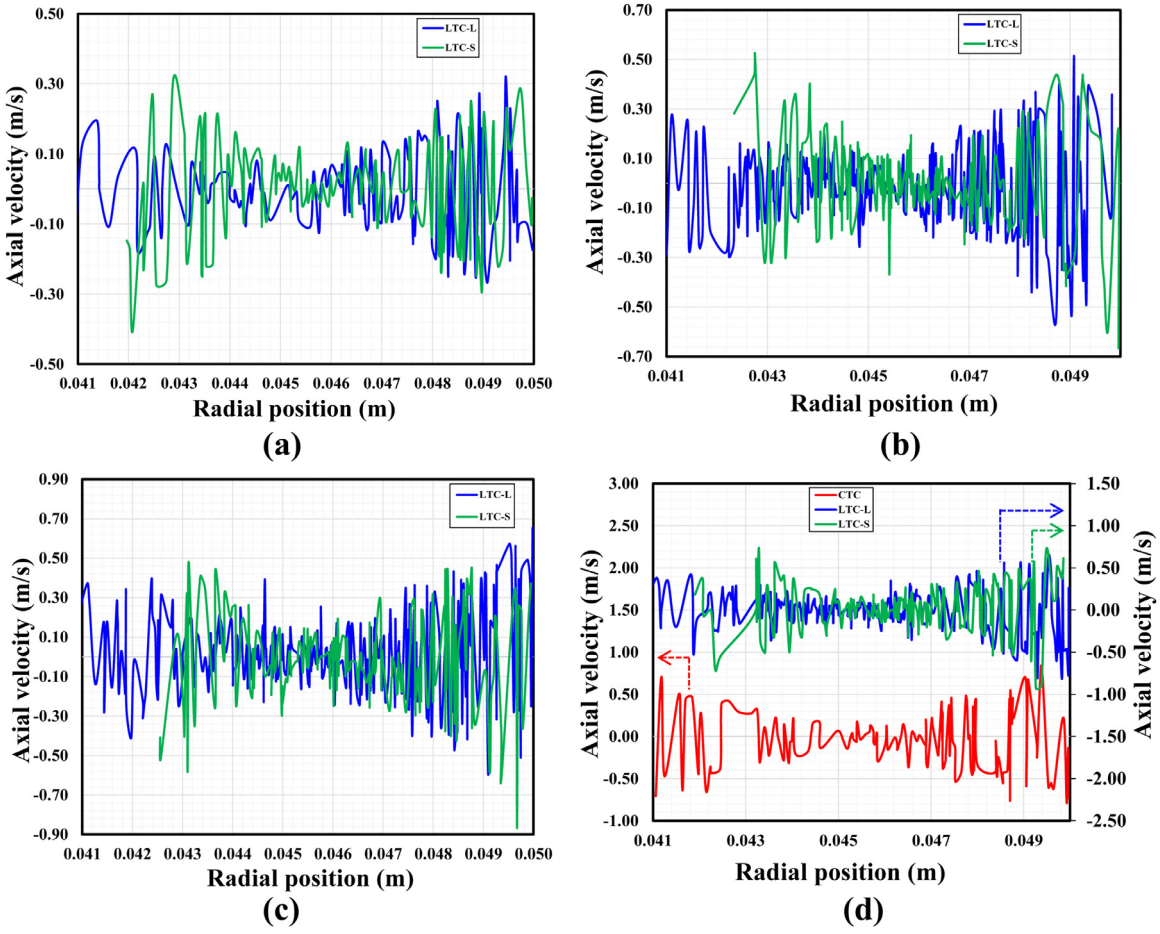

Figure 8. Axial velocity along radial position at: (a) 300 rpm; (b) 600 rpm; (c) 800 rpm; and (d) 1000 rpm.

change of particle axial velocity component in radial direction is shown in Figure 8, which is quantitatively consistent with the results as shown in Figure 7. One can argue that when the particles are entrapped in the core of the vortices, they are mainly affected by the vortices and the embedded turbulent eddies. Thus, the dispersion will mainly occur in the vortices. It is interesting to note here that in Figure 8, when comparing the vector marked by green line (i.e., the axial velocity in small gap) with the one marked by blue line (i.e., axial velocity in large gap), high axial velocity is found to occur at the region with small gap near the inner cylinder. However, the results shown in Figure 3 suggest that particle velocity magnitude is relatively high in the region with the large gap. This may be the consequence of the circumferential flow passing the narrowest gap between the rotating inner cylinder and the outer cylinder, generating local circulation eddies which may generate a high pressure zone and thus high particle velocity, as shown in Figure 5. Subsequently,

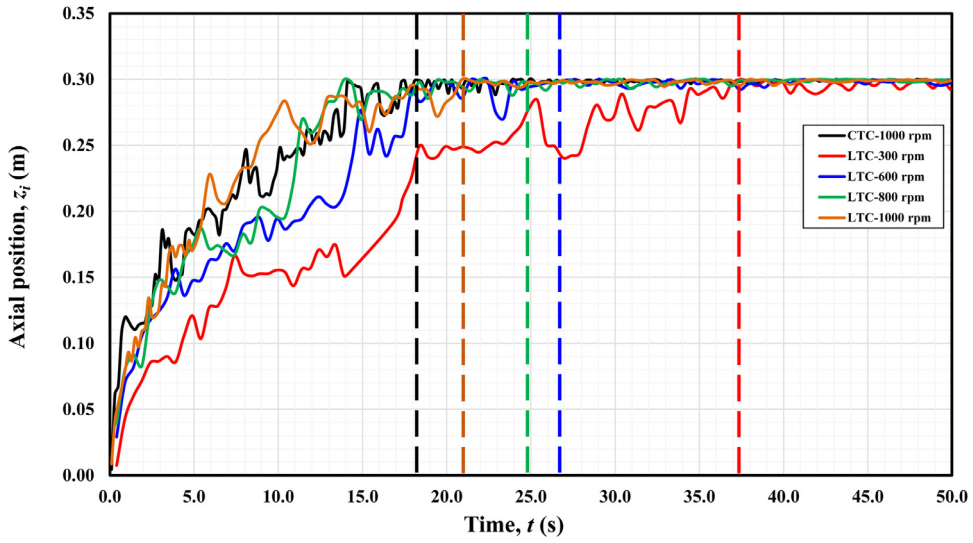

Figure 9. Particle axial dispersed position with the vertical dash lines denoting the minimum time required for particles to reach the outlet in each case.

the drag force increases as the result of the increase in slip velocity between the particle and local reactant liquid. These results have the implication that the LTC can be effective for particle classification. Actually, in the study of Kim *et al.* [18], they investigated particle movement with a constant density of 1760 kg/m^3 in a TC reactor, and they have found that large particles with the size up to 0.7 mm sink to the bottom through bypass flow while small particles (at least 0.05 mm) stay trapped in the core. In the study of Ohmura *et al.*'s [19], they observed that large particles concentrate near the edges of vortex. However, for particle classification, not only particle size but also particle density plus local particle concentration should be taken into account. These joint factors should be further studied with the loading capacity of Taylor vortices by introducing the Stokes loading factor.

3.4. Particle dispersion in axial direction

Figure 9 shows the scattered particle axial positions varying with time. At the rotational speed of 300 rpm, the time required to reach the farthest axial position measured from the bottom of the LTC is greater than 38 s, while when increasing the rotational speed, less time is needed for the particles to disperse to the same distance. It can be seen from the figure that the time reduces to 21 s in the LTC at the rotational speed at 1000 rpm while the time is only 18 s in the CTC. Such longer particle travelling time in the LTC indicates that the deformed Taylor vortices may have a longer and stronger impact on the particle dispersion than those in the CTC. The deformed Taylor vortices due to the inner cylinder change can be characterized by the energy dissipation rate shown in Figure S1 of the supplementary material. This result can also be found in Gu *et al.*'s [41] study. They found that fractal impellers can produce jet flows, breaking up the trailing vortices into smaller ones, then turbulence can be enhanced. However, it is interesting to note that the particle dispersion fluctuation in the LTC is more apparent than that in the CTC, indicating that particle dispersion is locally stochastic, and turbulent eddies fails to interact well with those particles.

In order to quantitatively estimate particle dispersion in the axial direction, an "effective particle diffusion coefficient" is used as

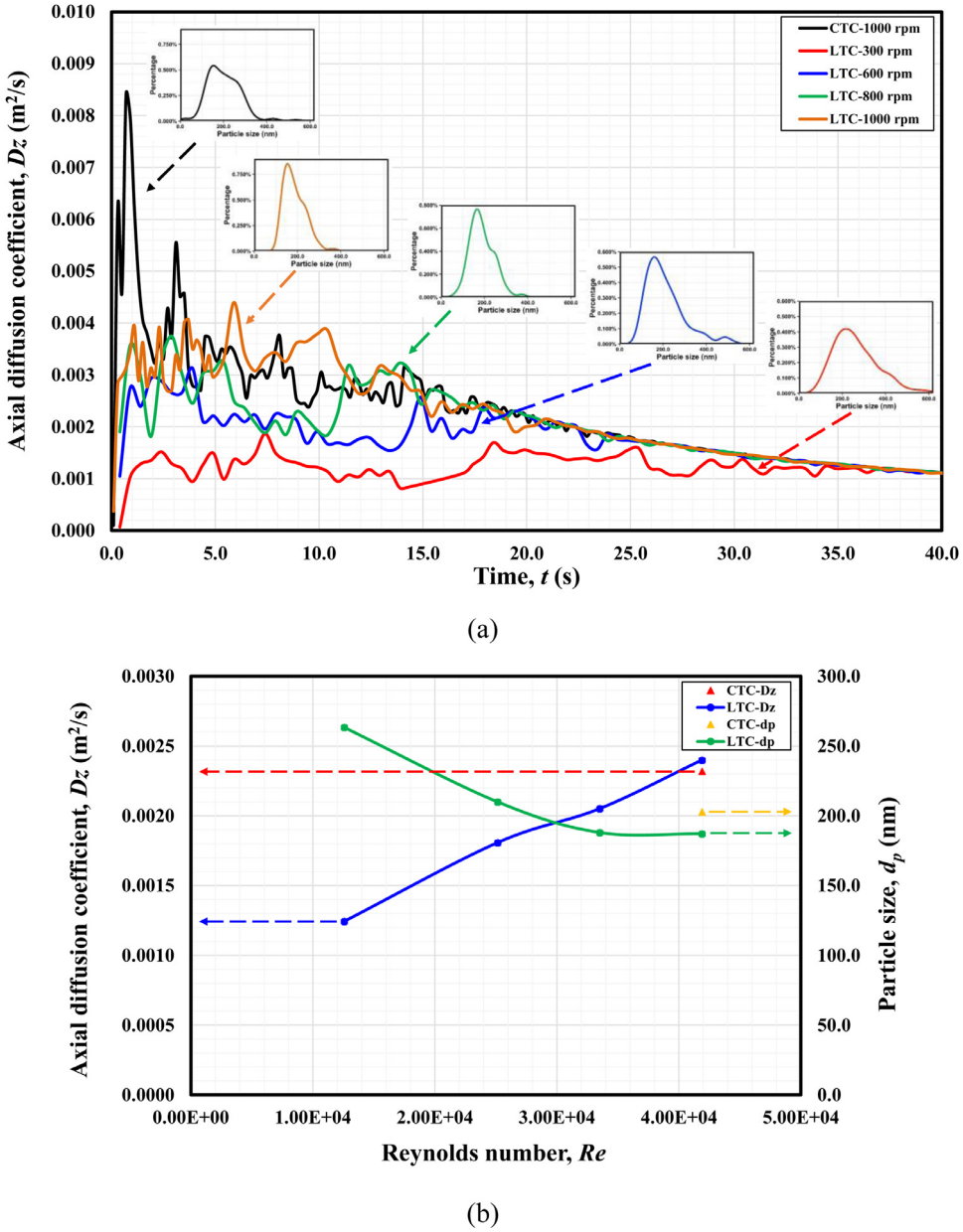

Figure 10. (a) Diffusion coefficient distribution and particle size distribution; and (b) Diffusion coefficient and particle size (D50) at different Reynolds numbers.

suggested by Rudman [42]. It should be pointed out that this coefficient can also indicate the global mixing performance. In the experiment of Liu *et al.* [27], the TC reactor was aligned vertically, and the particles were entrained in the axial direction by the Taylor vortices formed in the reactor. Thus, the axial diffusion is appropriate to characterize global mixing. In order to ensure for a reliable estimation of the particle axial dispersion, a large number of particles should be tracked. In this study, more than 1,000 particles (parcels) were injected in the computational domain, whose trajectories were tracked based on the modelling as described in Section 2. The particle axial dispersion is thus calculated using Equation (20), given by

$$D_z = \lim_{t\to\infty} \frac{1}{N}\sum \frac{\left(z_i(t) - z_i(0)\right)^2}{2t} \tag{20}$$

where Dz is the diffusion coefficient, N is the total number of particles tracked, $z_i(0)$ is the initial position of particles, and $z_i(t)$ is the axial position of the i^{th} particle at time step t.

Figure 10 (a) shows the axial diffusion coefficient as the function of time. Also, the particle size distribution at each condition, collected based on the actual experimental data at the time after reaching the average residence time, is displayed for reference. As particles are entrained away from their initial position, Dz increases first, following by a dropping down, and then level off with time. By observing the results of particle size distribution, it can be seen that the uniform particle size with a relatively narrow size distribution is achieved in the LTC at high rotational speed. However, in the CTC, particles size shows a rather broad size distribution, implying that the more time is needed for all particles to reach the same level, corresponding to the greater fluctuation of dispersion coefficient.

Some previous studies have investigated the relationship between the axial dispersion and the Reynolds number. Moore and Cooney [43] suggested that for the wavy vortex flow, Dz is proportional to $Re^{1.05}$. Rudman [42] found that for the modulated wavy vortex flow, Dz is proportional to Re, while Tam and Swinney [44] indicated that for turbulent flow in the Taylor-Couette system, Dz is proportional to Re^{β}, where β is mainly dependent on the radius ratio. It can be seen that Dz will change non-monotonically with Re for different flow patterns in the TC reactor. For our study, the relationship between Dz and Re is illustrated in Figure 10 (b), which is consistent with those aforementioned studies, where the diffusion coefficient increases with the increase of Reynolds number but the value of the coefficient for the CTC is smaller than that in the LTC. It should be noted that the average particle size (D50) obtained shows an opposite trend with the respect to the diffusion coefficient. As Dz can serve as an indicator of global mixing, the good mixing condition is achieved at high rotational speed, especially in the LTC. Thus, the use of the LTC can improve the particle synthesis process, as indicated by the greater Dz and being consistent with the previous study of Nemri *et al.* [45]. They indicated the existence of two types of mixing in the TC reactor, inter-vortex mixing and intra-vortex mixing. Inter-vortex mixing depends on the local turbulence and vortices such as the local impinging jet flows while intra-vortex mixing is dominated by the embedded turbulent eddies. An effective dispersion behaviour will create a good mixing condition for chemical reaction, intensifying particle dispersion process.

It should be noted that particle size not only depends on the synthesis reaction condition but also the formed particles are influenced by shear force exerted on particle surface. Figure 11 shows the distribution of the shear strain rate along the middle vertical line in the gap, and this line is across the centres of all the Taylor vortices in the TC reactor. The blue line represents the large gap region, and the green line denotes the small gap region in the LTC. The maximum shear strain rate appears at the inward and outward impinging jet regions. Also, vortex induced shear increases with increase in the rotational speed. Although the shear strain rate in the CTC is

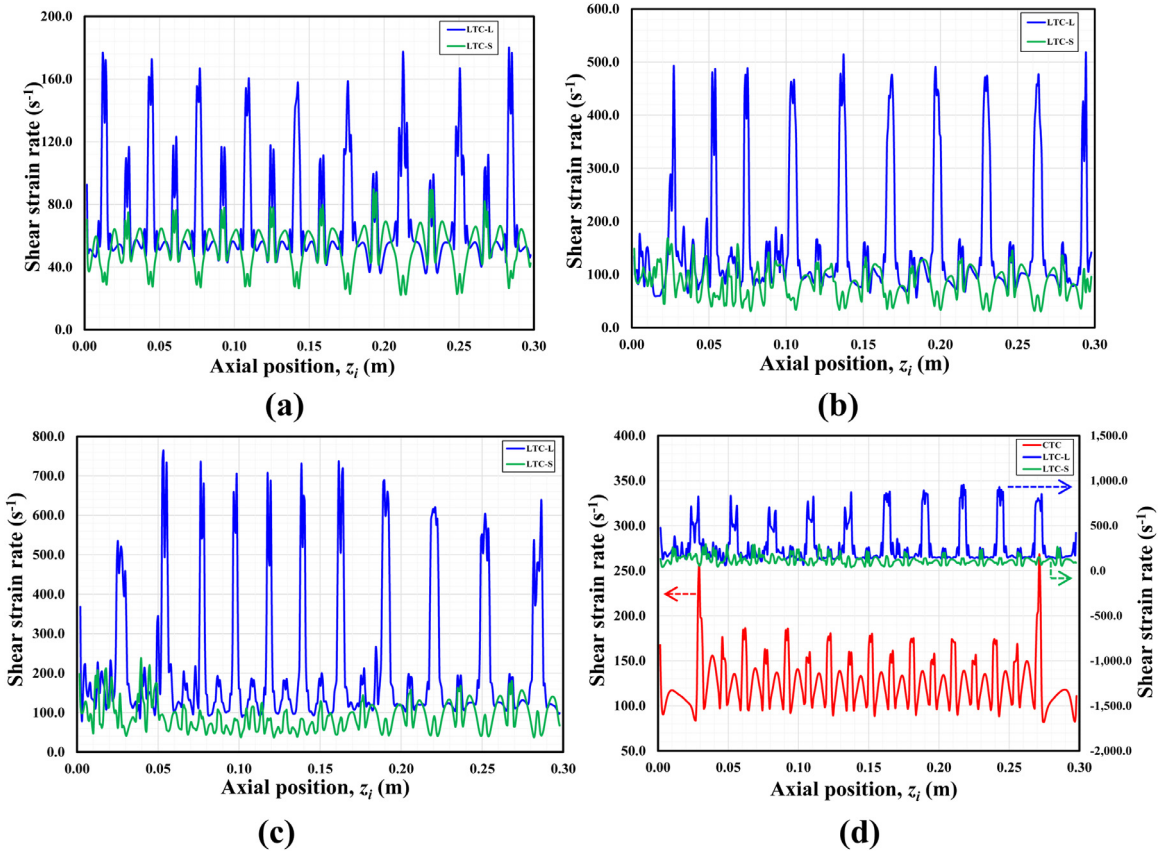

Figure 11. Shear strain rate along axial position at: (a) 300 rpm; (b) 600 rpm; (c) 800 rpm; and (d) 1000 rpm.

distributed more evenly than that in the LTC, the volume-average shear strain rate in the CTC is much smaller than that in the LTC. This indicates that the alteration of the cross-sectional profile of inner cylinder can effectively enhance the turbulence eddy induced shear. Due to the periodic variation of gap size in the LTC, turbulence intensification can be obtained, resulting in the generation of more turbulent eddies. Consequently, such turbulent shear acts on particles, curbing the particle growth so as to control the particle size.

4. Conclusions

Effect of hydrodynamic heterogeneity on particle dispersion in a Taylor-Couette flow (TC) reactor with variable configurations of inner cylinder has been investigated using CFD modelling. Tracking of particle motion was based on the Eulerian-Lagrangian approach, where the reactant solution phase was solved in the Eulerian reference frame, while the particle dispersion was calculated by tracking a large number of barium sulfate particle with consideration of the interfacial forces acting on particles and adopting the actual particle properties measured from particle synthesis experiments. The main observations and results are summarized as follows:

(1) The simulation reveals that particle dispersion is significantly enhanced by increasing the inner cylinder rotational speed, characterized by particle distribution for given the same particle residence time. Particles with high velocity magnitude tend to distribute in the large gap regions in the LTC, likely being attributed to the entrainment of particles by the impinging jet flows towards these regions, and the gradually decrease gap for the LTC, where the flow in circumferential experiences an expansion following by a contraction. The calculated particle trajectories in both the LTC and CLC exhibit helical movements, entrapped by Taylor vortices when judging the Stokes number.
(2) Particle dispersion in radial direction affects particle classification by presenting different particle axial velocities. It indicates that there exists a separation strap of the particles inside and outside the vortices. Such axial velocity distribution may be due to the circumferential flow, generating local circulation eddies.
(3) Particle dispersion in axial direction, which can be seen as an indicator of the global mixing occurring in the TC reactor, has also been investigated. The axial dispersion coefficient *Dz* was numerically calculated from Lagrangian tracking simulation, revealing a significant impact of the local turbulent impinging jet flows around the Taylor vortices on the mixing. The greater *Dz*, an indicator of a good mixing condition is achieved at high rotational speed, especially in the LTC. The distribution of the calculated *Dz* is found to be similar to the shape of particle size distribution based on the experimental results [27]. Besides narrow distribution, particle size is also relatively small in the LTC. Such uniform and small particle size is related to turbulent eddy shear, as shear force acting on particle surface can control particle to grow isotropically and to present more regular morphology.

Declaration of Competing Interest

The authors declare that they have no known competing financial interests or personal relationships that could have appeared to influence the work reported in this paper.

Acknowledgement

The authors acknowledge the financial support by National Natural Science Foundation of China (NSFC) through the grant (Nos. 21761132026, 21576141, 21606259, 91852205, 11961131006, 11988102), University of Nottingham Ningbo China (UNNC) Li Dak Sam Innovation Fellowship, Guangdong Provincial Key Laboratory of Turbulence Research and Applications (2019B21203001), Guangdong-Hong Kong-Macao Joint Laboratory for Data-Driven Fluid Mechanics and Engineering Applications (2020B1212030001).

References

[1] Serra T, Colomer J, Casamitjana X. Aggregation and breakup of particles in a shear flow. Journal of Colloid and Interface Science 1997;187(2):466–73.
[2] Bubakova P, Pivokonsky M, Filip P. Effect of shear rate on aggregate size and structure in the process of aggregation and at steady state. Powder Technology 2013;235:540–9.
[3] Mayra QP, Kim WS. Agglomeration of Ni-Rich hydroxide in reaction crystallization: Effect of Taylor vortex dimension and intensity. Crystal Growth & Design 2015;15(4):1726–34.
[4] Shen P, Yeung PK. Fluid particle dispersion in homogeneous turbulent shear flow. Physics of Fluids 1997;9(11):3472–84.
[5] Li J, Zeng XA, Brennan CS, Chen XD. Micron-size lactose manufactured under high shear and its dispersion efficiency as carrier for Salbutamol Sulphate. Powder Technology 2019;358:39–45.
[6] Snyder HA. Experiments on the stability of spiral flow at low axial Reynolds numbers. Proceedings of the Royal Society of London. Series A. Mathematical and Physical Sciences. 1962;265(1321):198–214.
[7] Lathrop DP, Fineberg J, Swinney HL. Transition to shear-driven turbulence in Couette-Taylor flow. Physical Review A 1992;46(10):6390.
[8] Ehrl L, Soos M, Wu H, Morbidelli M. Effect of flow field heterogeneity in coagulators on aggregate size and structure. AIChE journal;56(10):2573-2587.
[9] Vaezi V, Oh ES, Aldredge RC. High-intensity turbulence measurements in a Taylor-Couette flow reactor. Experimental thermal and fluid science 1997;15(4):424–31.
[10] Wang L, Olsen MG, Vigil RD. Reappearance of azimuthal waves in turbulent Taylor–Couette flow at large aspect ratio. Chemical engineering science 2005;60(20):5555–68 Oct 1.
[11] Tokgoz S, Elsinga GE, Delfos R, Westerweel J. Spatial resolution and dissipation rate estimation in Taylor–Couette flow for tomographic PIV. Experiments in fluids 2012;53(3):561–83.
[12] Marchisio DL, Barresi AA. CFD simulation of mixing and reaction: the relevance of the micro-mixing model. Chemical Engineering Science 2003;58(16):3579–87.
[13] Grossmann S, Lohse D, Sun C. Velocity profiles in strongly turbulent Taylor-Couette flow. Physics of fluids 2014;26(2):025114.
[14] Bazilevs Y, Akkerman I. Large eddy simulation of turbulent Taylor–Couette flow using isogeometric analysis and the residual-based variational multiscale method. Journal of Computational Physics 2010;229(9) 3402-3014.
[15] Chouippe A, Climent E, Legendre D, Gabillet C. Numerical simulation of bubble dispersion in turbulent Taylor-Couette flow. Physics of Fluids 2014;26(4):043304.
[16] Wang L, Vigil RD, Fox RO. CFD simulation of shear-induced aggregation and breakage in turbulent Taylor–Couette flow. Journal of colloid and interface science 2005;285(1):167–78.
[17] Dutta PK, Ray AK. Experimental investigation of Taylor vortex photocatalytic reactor for water purification. Chemical Engineering Science 2004;59(22-23):5249–59.
[18] Kim JS, Kim DH, Gu B, Yang DR. Simulation of Taylor–Couette reactor for particle classification using CFD. Journal of crystal growth 2013;373:106–10.
[19] Ohmura N, Suemasu T, Asamura Y. Particle classification in Taylor vortex flow with an axial flow. InJournal of Physics: Conference Series. IOP Publishing; 2005. p. 009.
[20] Jung WM, Kang SH, Kim KS, Kim WS, Choi CK. Precipitation of calcium carbonate particles by gas–liquid reaction: Morphology and size distribution of particles in Couette-Taylor and stirred tank reactors. Journal of Crystal Growth 2010;312(22):3331–9.
[21] Nguyen AT, Kim JM, Chang SM, Kim WS. Phase Transformation of Guanosine 5-Monophosphate in Continuous Couette– Taylor Crystallizer: Experiments and Numerical Modeling for Kinetics. Industrial & engineering chemistry research 2011;50(6):3483–93.
[22] Nguyen AT, Joo YL, Kim WS. Multiple feeding strategy for phase transformation of GMP in continuous Couette–Taylor crystallizer. Crystal growth & design 2012;12(6):2780–8.
[23] Kim JM, Chang SM, Chang JH, Kim WS. Agglomeration of nickel/cobalt/manganese hydroxide crystals in Couette–Taylor crystallizer. Colloids and Surfaces A: Physicochemical and Engineering Aspects 2011;384(1-3):31–9.
[24] Thai DK, Mayra QP, Kim WS. Agglomeration of Ni-rich hydroxide crystals in Taylor vortex flow. Powder Technology 2015;274:5–13.
[25] Kim JE, Kim WS. Synthesis of Core–Shell Particles of Nickel–Manganese–Cobalt Hydroxides in a Continuous Couette-Taylor Crystallizer. Crystal Growth & Design 2017;17(7):3677–86.
[26] Nemri M, Climent E, Charton S, Lanoe JY. Ode D. Experimental and numerical investigation on mixing and axial dispersion in Taylor–Couette flow patterns. Chemical Engineering Research and Design 2013;91(12):2346–54.
[27] Liu L, Yang X, Li G, Huang X, Xue C. Shear controllable synthesis of barium sulfate particles using lobed inner cylinder Taylor-Couette flow reactor. Advanced Powder Technology 2020;31(3):1088–99.
[28] Liu RJ, Xiao R, Ye M, Liu Z. Analysis of particle rotation in fluidized bed by use of discrete particle model. Advanced Powder Technology 2018;29(7):1655–63.

[29] Marocco L, Inzoli F. Multiphase Euler–Lagrange CFD simulation applied to wet flue gas desulphurisation technology. International Journal of Multiphase Flow 2009;35(2):185–94.
[30] Stone L, Hastie D, Zigan S. Using a coupled CFD–DPM approach to predict particle settling in a horizontal air stream. Advanced Powder Technology 2019;30(4):869–78.
[31] ANSYS FLUENT 18.0. User Guide. © ANSYS Inc; 2018.
[32] Yakhot VS, Orszag SA, Thangam S, Gatski TB, Speziale CG. Development of turbulence models for shear flows by a double expansion technique. Physics of Fluids A: Fluid Dynamics 1992;4(7):1510–20.
[33] Morsi SA, Alexander AJ. An investigation of particle trajectories in two-phase flow systems. Journal of Fluid mechanics 1972;55(2):193–208.
[34] Pirro D, Quadrio M. Direct numerical simulation of turbulent Taylor–Couette flow. European Journal of Mechanics-B/Fluids 2008;27(5):552–66.
[35] Fehrenbacher N, Aldredge RC, Morgan JT. Turbulence structure in a Taylor–Couette apparatus. Experimental thermal and fluid science 2007;32(1):220–30.
[36] Haut B, Amor HB, Coulon L, Jacquet A, Halloin V. Hydrodynamics and mass transfer in a Couette–Taylor bioreactor for the culture of animal cells. Chemical Engineering Science 2003;58(3-6):777–84.
[37] Li G, Yang X, Ye H. CFD simulation of shear flow and mixing in a Taylor–Couette reactor with variable cross-section inner cylinders. Powder Technology 2015;280:53–66.
[38] Soos M, Wu H, Morbidelli M. Taylor-Couette unit with a lobed inner cylinder cross section. AIChE journal 2007;53(5):1109–20.
[39] Qiao J, Deng R, Wang CH. Particle motion in a Taylor vortex. International Journal of Multiphase Flow 2015;77:120–30.
[40] Crowe CT, Troutt TR, Chung JN. Numerical models for two-phase turbulent flows. Annual Review of Fluid Mechanics 1996;28(1):11–43.
[41] Gu D, Ye M, Wang X, Liu Z. Numerical investigation on mixing characteristics of floating and sinking particles in a stirred tank with fractal impellers. Journal of the Taiwan Institute of Chemical Engineers 2020;116:51–61.
[42] Rudman M. Mixing and particle dispersion in the wavy vortex regime of Taylor–Couette flow. AIChE journal 1998;44(5):1015–26.
[43] Moore CM, Cooney CL. Axial dispersion in Taylor-Couette flow. AIChE Journal 1995;41(3):723–7.
[44] Tam WY, Swinney HL. Mass transport in turbulent Couette-Taylor flow. Physical Review A 1987;36(3):1374.
[45] Nemri M, Charton S, Climent E. Mixing and axial dispersion in Taylor–Couette flows: the effect of the flow regime. Chemical Engineering Science 2016;139:109–24.